# Initial Findings in Full-Shell Active Optics

Jacqueline Davis and Stephen Bongiorno

NASA Marshall Space Flight Center, Huntsville, AL, 35812

## ABSTRACT

The realization of active full-shell x-ray optics will provide ground-breaking capability for future missions. Future X-ray missions, such as Lynx, require high angular-resolution, large effective area, and as wide a field of view (FOV) as possible. It is currently not possible to perform high-resolution imaging of both wide and narrow FOVs with a single X-ray telescope. In this paper, we discuss the use of actuators to switch the optical surface of full-shell x-ray optics between prescriptions optimized for narrow-field and wide-field viewing, as well as correct for low-spatial-frequency errors in the optics. Previously, a pathfinder was developed using finite-element modeling (FEM). Using a combination of the model's influence functions, the capacity of active full-shell optics was shown to switch between prescriptions with 92% accuracy. Another benefit of the analytical pathfinder was its ability to correct low-spatial frequency errors, which comprise a large percentage of the MSFC full-shell x-ray optics root-mean-square (RMS) slope error. In order to verify the pathfinder, a surface-parallel actuator was bonded to a nickel-replicated coupon. After the actuator was bonded to the coupon, the slope of the surface was measured while the actuator was activated. The proof-of-concept demonstrator development, the influence function data, and the resulting implications on the analytical pathfinder are reported and discussed.

**Keywords:** active optics, grazing-incidence, x-ray, optics

## 1. INTRODUCTION

The performance of grazing-incidence X-ray telescopes are characterized in terms of their imaging quality over a given FOV and their effective area. In general, the on-axis effective area is used to characterize the collecting power of an X-ray optic. The telescope's ability to image extended sources is also determined by the angular-resolution of the optical assembly and by the variation in effective area with the off-axis angle. As an X-ray source moves off-axis, the effective area decreases, which causes a loss of sensitivity in the peripheral regions of the telescope's field of view (FOV).[2] The work described here provides a solution for improving the angular-resolution of single and assembled optics modules, and provides a means to adjust the prescription to meet multiple mission needs with a single telescope.

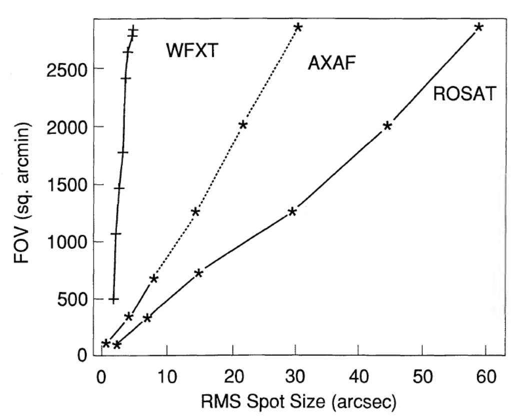


Figure 1: Burrows[1] plots the total available FOV as a function of the average image quality for the Wide Field X-Ray Telescope (WFXT), AXAF (before optimization), and ROSAT. The dotted line represents field angles which detectors do not cover.

Wolter-Schwarzschild and Wolter I designs yield perfect images on-axis in theory, however, the aberrations increase with field angle. Because of this, the telescope prescription must be tailored to meet the science goals. Burrows compared the image quality of an optimized polynomial prescription of the Wide Field X-ray Telescope (WFXT) in Figure 1 to the optics in Chandra (previously

Further author information: (Send correspondence to 320 Sparkman Drive, Huntsville, AL 35805)
J.M.D.: E-mail: jacqueline.m.davis@nasa.gov, Telephone: 1 256 961 7445

named AXAF) and ROSAT.[1] A solution for a high-angular-resolution, wide-FOV prescription is possible if perfect on-axis resolution.

Chandra achieved on-axis sub-arcsecond angular resolution with four nested pairs of full-shell mirrors that were directly fabricated out of glass, ranging in thickness between 16-24 mm.[3] The goal for the next generation of X-ray telescope is to achieve the same angular resolution while increasing the FOV by manufacturing much thinner (∼0.5 mm) mirrors; this allows for greater nesting of mirror pairs and larger effective area while simultaneously reducing mass per collecting area.[4] Thinner optics are more susceptible to distortions and require groundbreaking technological advancements in optical fabrication;[5] the work described here will provide a means to improve angular-resolution of single and assembled optics.

The X-ray optics group at MSFC has developed a manufacturing process over the past 25 years using electroformed nickel replication to produce full-shell, grazing-incidence mirrors (shown in Figure 2). The shells are electro-deposited onto a figured mandrel and released in a chilled water bath. The shells are almost 100 times thinner than the Chandra shells which makes them more susceptible to figure errors.[6]

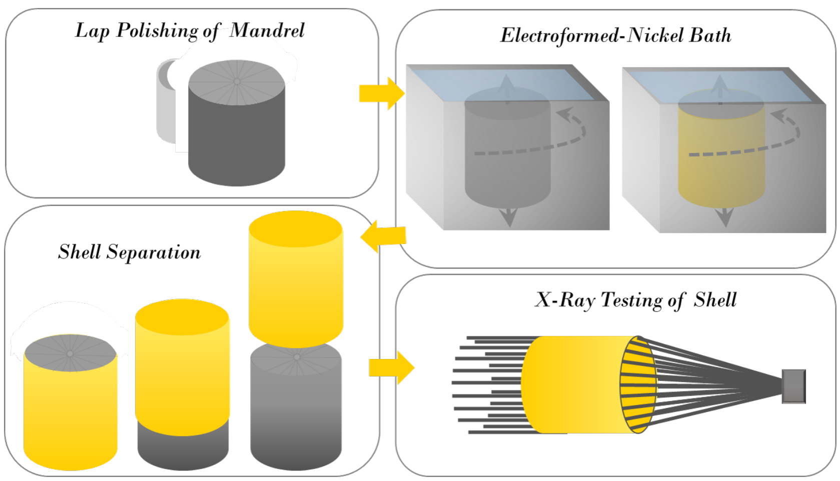


Figure 2: Simplified overview of MSFC full-shell optics replication process.

The mirror modules in ART-XC, which flew aboard the Spectrum-Rontgen-Gamma Observatory, were manufactured at MSFC using the electro-formed nickel replication process. The telescope consist of 7 identical co-aligned mirror modules, each nesting 28 mirror shells (Figure 3).

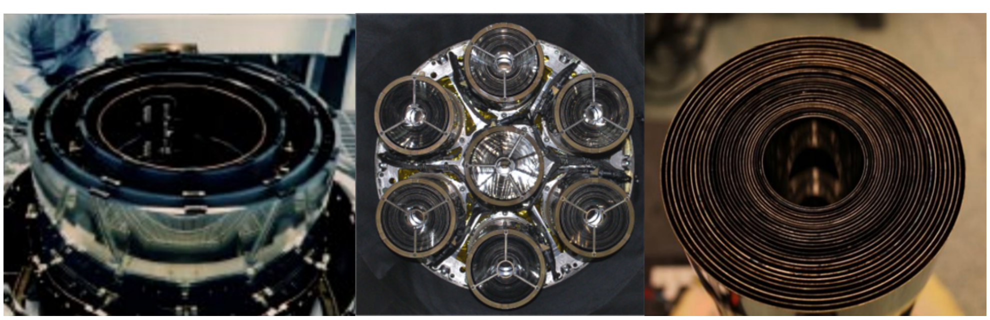

Figure 3: left: Chandra mirror assembly (120 cm diameter) with 4 mirror pairs; center: ART-XC telescope with 7 identical mirror modules;[7] right: single ART-XC mirror module (15 cm) with 28 nested mirror shells fabricated at MSFC with replication process.

ART-XC optics shows the technology is moving towards the highly nested specifications set by the Lynx concept study for the next generation X-ray optics to have ∼150 shells within a 3 m diameter (Figure 4). The

ART-XC mirror module has an effective area per volume of approximately 10 times that of Chandra; however, the angular resolution is only 25" HPD.[8] Although the replicated-nickel process has proven successful at creating efficiently nested shells, work needs to be done to improve angular resolution.

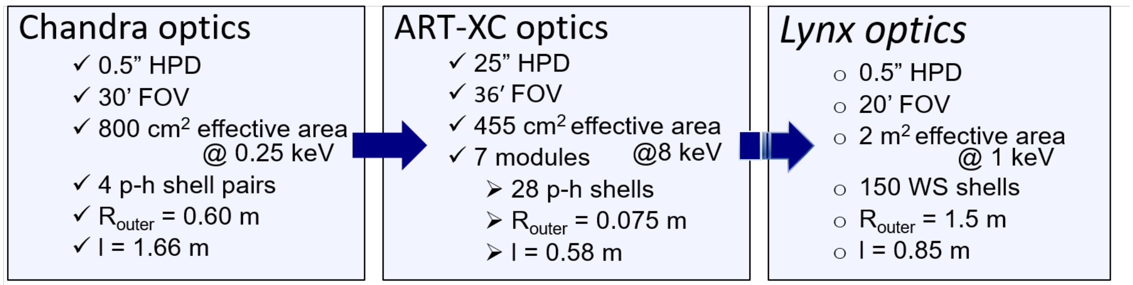


Figure 4: Trend of mission specifications for grazing-incidence optics.

Beyond improving figure error, the objective of this work is to use active full-shell X-ray optics to switch between a wide field prescription and a narrow field prescription. The concept of using actuators to switch full-shell X-ray optics between prescriptions is novel and will enable a single observatory to possess the ability to collect high-resolution imaging in a narrow field as well as a wide field. Currently, the only way to have both optimized narrow and wide fields of view (FOVs) would require multiple telescopes (either on the same payload or launched separately).

The objective of this paper is to discuss advancements and lessons learned since an initial proof-of-concept of the active full-shell X-ray optics discussed in our 2016 SPIE proceeding.[9] The resulting analytical pathfinder is a novel concept with the capacity to switch between optical prescriptions as well as correct low-order figure errors.[9]

## 2. ANALYTICAL PATHFINDER

### 2.1 Full-Shell Pathfinder Criterion

In order to explore the concept of switching prescriptions and low-order figure error correction, a trade study was performed using finite-element modeling (FEM).[9] During the study, the actuator configuration pattern was changed while the shell mirror specifications remained constant. The capacity of each configuration to perform error reduction and prescription change was based on two set deformations:

1. Manufacturing error: error on the optical surface of the nickel-replicated X-ray shells, measured with the Vertical Long Trace Profilometer (VLTP);[10] the deformation was chosen because its magnitude and figure error was determined to be a typical of optics manufactured at MSFC.
2. Prescription change: difference between Wolter I and Wolter Schwarzchild; future work will cover a Wolter I to a polynomial prescription.

Configurations of actuators were analyzed using FEMs of actuators bonded to full-shell grazing-incidence optics. The models were developed using three actuator configurations: surface-normal, zonal-meniscus and surface-parallel array actuators are shown in Figure 5; for each configuration type, models were created with varying number of actuators. A load was applied to each actuator in each model, and the deformation on the optical surface was exported. A combination of influence functions (IFs) for each model was used to fit to the manufacturing errormap and the prescription shape change.

The correctability analysis showed that the models where the actuators are placed parallel to the optical surface, or surface-parallel actuators, showed a higher fidelity fit to both manufacturing error and prescription switching. Although both zonal-meniscus and surface-parallel array (SPA) contain surface-parallel actuators, the SPA actuators have minimal aperture obstruction, which is a key design feature in the design of X-ray optics.

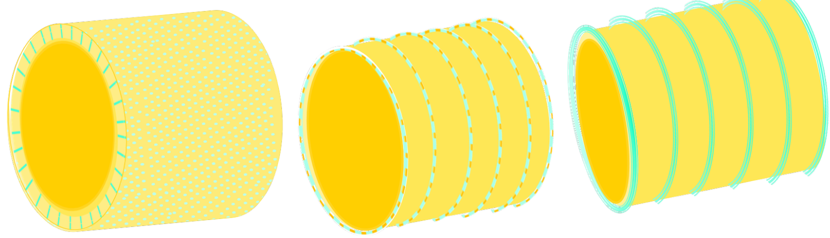

Figure 5: Analytical models: left: surface-normal actuators between 2 nested full-shell x-ray optics; center: zonal-meniscus actuators on full-shell x-ray optic; right: surface-parallel array (SPA) full-shell x-ray optic.

Moving forward, the actuator configuration with six bands of SPA actuators will be called the pathfinder. Out of the models analyzed, it showed the best capacity to correct manufacturing error and create the shape necessary to switch the mirror's prescription. Figure 6 shows the six IFs of the bands of SPA actuators.

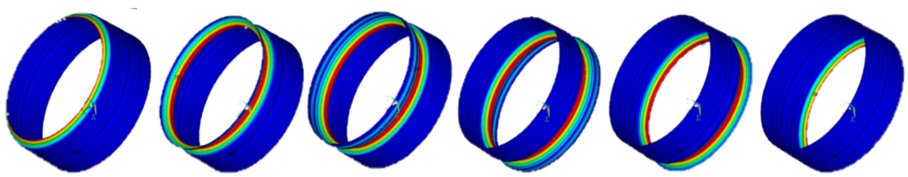

Figure 6: SPA influence function when placed around full-shell mirror at 6 equidistant bands.

The correctability of the pathfinder is shown in Figure 7. The upper left plot shows an azimuth of the manufacturing error of a nickel-replicated, grazing-incidence optic. After using the IFs from Figure 6 to do a least-squares-fit (LSF) to the manufacturing error, the remaining theoretical residual error is plotted in the lower left of Figure 7. The upper right plot is the difference between a Wolter I prescription and a Wolter Schwarzchild prescription, and the lower right plot shows a theoretical LSF using the pathfinder's IFs.

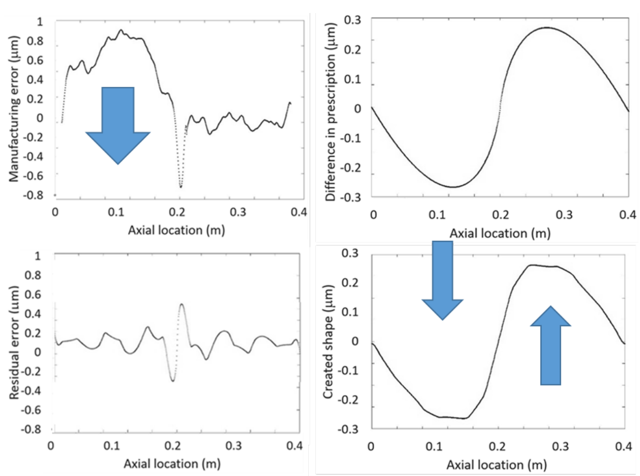


Figure 7: upper left: error of MSFC nickel-replicated optic; upper right: deformation necessary for prescription change; bottom left: analytical replication residual error; analytical deformation for prescription change.

The overall correctability analysis indicated that the ability to correct low-spatial frequency errors is significant. The prescription changes are low-spatial figure changes, and the reduction of low-spatial figure error comprises a large percentage of RMS slope error.

### 2.2 Sub-Scale Analysis

In moving towards the development of a sub-scale prototype, the main design feature is the capacity to induce low-spatial figure change. The biggest hurdle in developing an active optic is insuring the bonding of actuators has minimal effect on the optical quality of the mirror.

MSFC has previously developed a method to mimic the electro-formed nickel process on a sub-scale flat coupon. Ideally, the sub-scale prototype would consist of a SPA actuator bonded to a nickel-replicated coupon, however, these actuators are not COTS products. Lead zirconate titanate (PZT) sheet actuators were the most similar product that was readily available.

Because inducing large slope changes was the priority for the sub-scale prototype, zonal-meniscus actuation along with the PZT sheet actuators were pursued (Figure 8).

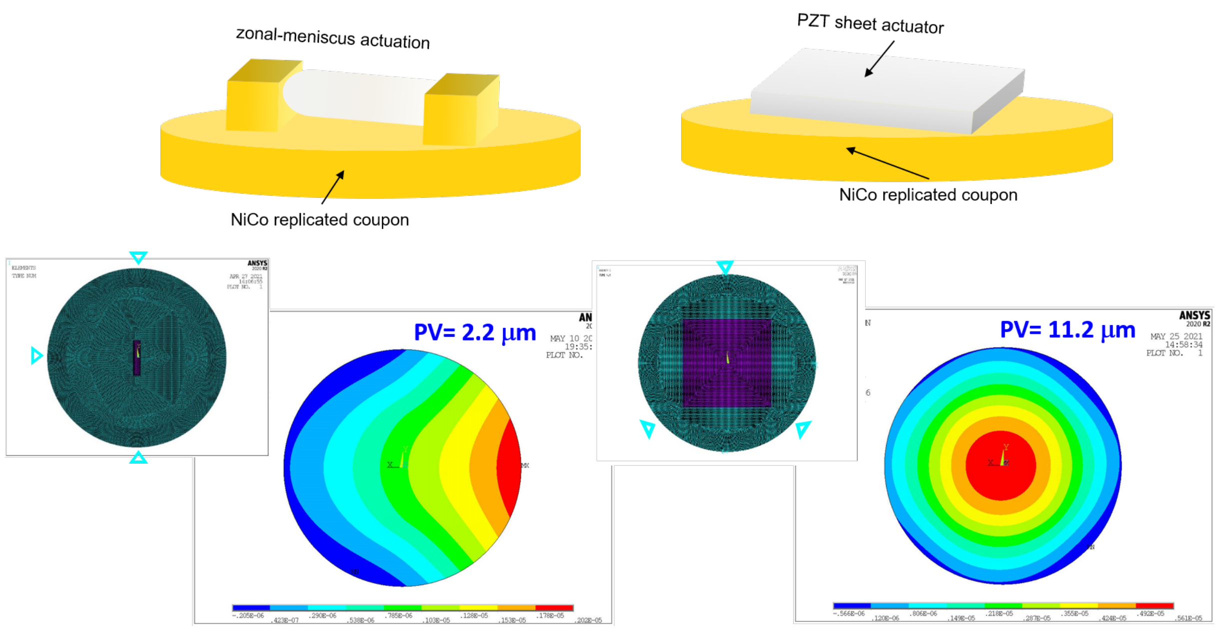


Figure 8: sub-scale prototype designs based on pathfinder analysis; left: zonal-meniscus; right: PZT sheet.

A FEM was created of each design configuration, varying the size and traits of the actuators. The results are shown above for each configuration that showed the most deformation with minimal obstruction away from the coupon. Because of its ease of manufacturability along with its larger deformation, the PZT sheet was chosen as the sub-scale prototype design.

### 2.3 Bonding Analysis

After determining the path forward with PZT sheet actuators, classical laminate theory (CLT) was used to determine piezo thickness and bond line thickness for the sub-scale optic. A 48 mm diameter, 254 $\mu$m thick nickel-replicated coupon was used for the model. Figure 9 shows a large slope change with any of the off-the-shelf sheet actuators, in particular for thicknesses less than 60 microns. Therefore, the PZT-5A actuator with a 267 $\mu$m thickness was chosen for the first sub-scale demonstrator due to its accessibility.

The CLT predicted that a bond line between 1 $\mu$m and 180 $\mu$m will produce between 0.533 $m^{-1}$ - 0.397 $m^{-1}$ curvature at maximum actuation. The relation is approximately linear. Scaled to 65V lab actuation voltage, the induced curvature is 0.098 $m^{-1}$ at the expected bond line thickness of 127 $\mu$m.

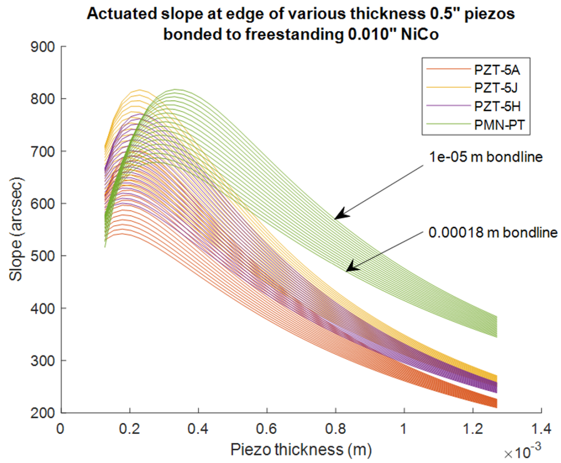


Figure 9: Slope induced for available actuator sheets, varying sheet thickness and bondline thickness.

## 3. SUB-SCALE NICKEL-REPLICATED OPTIC

A sub-scale active optic demonstrator was built to begin hardware demonstrations for active full-shell X-ray optics to validate bonding procedures. The demonstrator consisted of a 254 $\mu$m thick, 48 mm diameter nickel-cobalt flat optical coupon bonded to a 267 $\mu$m thick, 36.2 mm square sheet of piezo ceramic with unfilled Hysol EA9313. In the future, the bond line between the optical coupon and the piezo sheet will be regulated with spacers; however, in this demonstrator, it was not.

### 3.1 Bonding Process

Bonding layup of the optical coupon to the piezo is shown in Figure 10 on the left, and a description of the process is listed below.After the epoxy was cured, the bonded demonstrator was released and mounted on a three-point pseudo-kinematic magnet mount for optical testing, as shown in Figure 10 on the right.

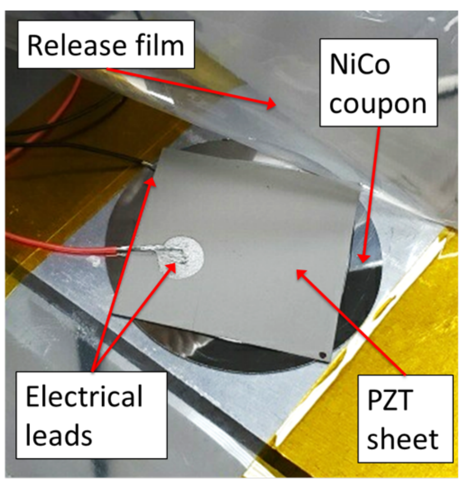


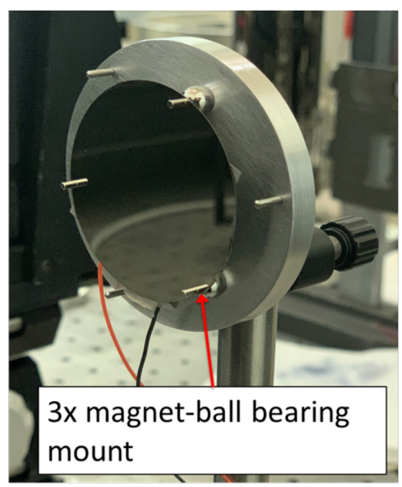


Figure 10: left: bonding process of PZT sheet to nickel-replicated coupon. right: active optic mounted on 3-point pseudo-kinematic mount.

- cleaved 70 mm square x 267 $\mu$m PZT-5A into 4 squares with diamond scribe
- bonded wire leads to PZT with conductive epoxy, cured at 140$^o$F for 15 min, as indicated by manufacturer

- clamped between aluminum
- bond coupon to PZT with unfilled Hysol EA9313
- covered optical surface and aluminum plate base with tape
- covered with cut square of plastic contamination bagging material as a release layer
- block of Ethylene-Vinyl Acetate (EVA) foam on top, covered with aluminum plate and clamped

### 3.2 Sub-Scale Optic Influence Function Results

Bonding a dissimilar material to the back of an optic creates distortions on the optical surface due to thermal mismatch during the curing process.[11] Clamping the foam opposite to the optic was an attempt to mitigate the bonding errors, however, the errors were severe. When using active optics, the actuators can reduce the optical error, however, in this case, the distortions made it difficult to get an optical measurement.

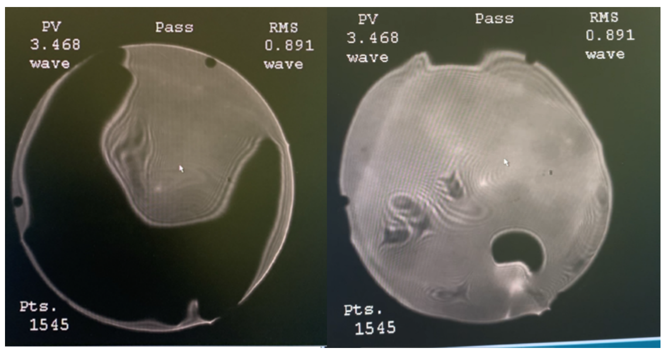


Figure 11: Zygo interferograms of active optic at 0V (left) and 65V (right).

Figure 11 shows two interferograms of the sub-scale active optic. The left shows the dropout data due to epoxy shrinkage; the right shows an improved interferogram after applying 65V to the actuator. Even though it was better, the image could not be resolved because of some print-through error due to both wire bonding sites, especially the buried negative lead.

Because an optical measurement was not possible, a Keyence laser displacement sensor was used to measure the IF of the active optic. The sub-scale demonstrator was scanned 35mm from the bottom of the optic with the Keyence LK-G10 laser displacement sensor with the actuator set to 0V and 65V. The two scans were subtracted to produced a 1-D IF, shown in Figure 12.

From the IF, we calculated the induced curvature at 65 V was 0.018 $m^{-1}$. CLT predicted the induced curvature would be 0.098 $m^{-1}$. This discrepancy may be due to misalignment of the coupon during measurement and error in the bond line thickness estimate. Both points will be addressed in future iterations.

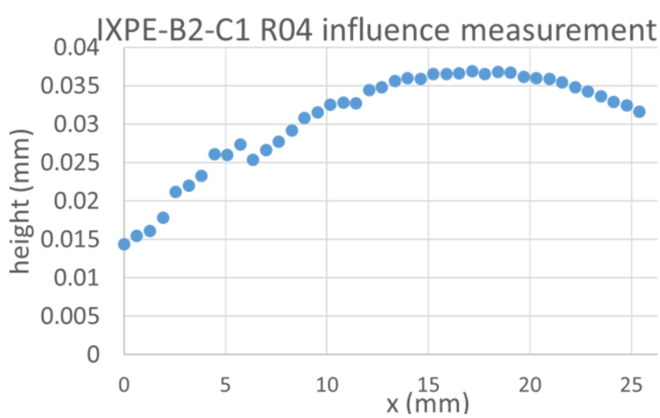


Figure 12: Influence function measured with Keyance Sensor.

The next step is to mitigate large print-through error. One path will be to reduce the size of the actuator, which will reduce the surface-area of the bond between the actuator and the optic.

# 4. SCALING UP TO AN ACTIVE FULL-SHELL X-RAY OPTIC

## 4.1 Bonding to Shell

After further studies to reduce bonding print-through error, the sub-scale design will be adapted to a full-shell active X-ray optics design. Initially, the actuators will be bonded to a stiffness ring, as shown in Figure 13. Next, a band of actuators will be bonded around the entire circumference of the shell. In both cases, the slope across the azimuth of the optic will be measured using the VLTP,[10] and the IFs will be calculated by collecting data while activating the actuators. The IF data will be used to compute the performance of the full design.

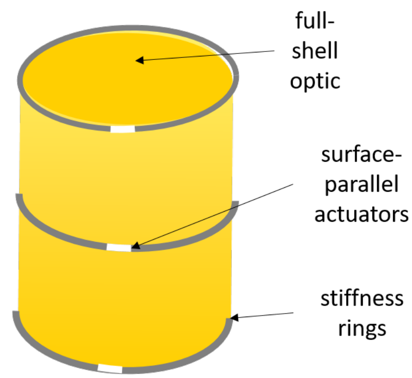


Figure 13: Diagram of demonstration of bonding actuators to full-shell.

## 4.2 Steps to Apply Active Full-Shell X-ray Optics to Future Missions

Future X-ray missions would like to extend Chandra's high-resolution imaging to wide-field surveys as well as extended sources. The goal for the next generation of X-ray telescope is to achieve 0.5 arcsecond HPD angular-resolution in the narrow field while staying below one arcsecond HPD in the wide field. Applying the active prescription switching concept to this allows a loosening of manufacturing tolerances in other areas. The actuators can be used to switch from a Wolter I for the tight on-axis requirement, then switch to a polynomial prescription, meeting the overall wide-field requirement.

In addition to optimizing the prescriptions, a larger FOV requires highly nested shells with thinner mirrors. Although the actuators do take up valuable real estate, the active full-shell X-ray optics concept will also create a type of "agile stiffness." Along with reducing the figure error, the active bands can reduce the flimsiness of the shells during handling, mounting and alignment procedures.

# 5. SUMMARY

The advancement of the nickel-replicated full-shell optics at MSFC have the ability to meet future X-ray mission needs. Both prescription switching and figure error correction can provide full-shell optics with improved angular resolution and the ability to meet multiple mission needs. Active X-ray optics can relieve tolerances in other manufacturing areas by switching between Wolter I and polynomial prescriptions. A polynomial prescription has a high angular-resolution across a wide FOV. Wolter I telescopes have extremely high resolution on-axis across a narrow field but have a low resolution at a wide field. Meeting these requirements at the same time would be much more difficult to achieve.

Another benefit of active full-shell optics is the ability to correct low-spatial frequency errors. Removing low-spatial frequency error, comprising the largest percentage of root-mean-square (RMS) slope error, other processes being developed at MSFC will have greater performance and more efficiency removing mid- and high-spatial frequency errors.

A sub-scale active X-ray optic was developed and tested. The bonding process was found to significant print-through error, and studies are currently under way to mitigate these errors. Planned follow-on efforts will include a grazing-incidence, full-shell prototype, which will be designed, modeled, built, and tested. The key design considerations are the shape of the IFs and its capacity to form the shape of prescription switching and reduce low-order spatial frequency manufacturing errors.

## REFERENCES


[1] Burrows, C., "Optimal grazing-incidence optics and its application to wide-field x-ray imaging," *The Astrophysical Journal* **392** (1992).

[2] Spiga, D., "Analytical computation of the off-axis effective area of grazing incidence x-ray mirrors," *Astronomy and Astrophysics* **505** (2009).

[3] Weisskopf, M., "An overview of the performance of the chandra x-ray observatory," *Exp. Astron.* **16**, 1–68 (2003).

[4] Gaskin, J., "Lynx x-ray observatory: an overview," *J. Astron. Telesc. Instrum. Syst.* **5** (2019).

[5] Davis (Roche), J., "Opto-mechanical analyses for performance optimization of lightweight grazing-incidence mirrors," in [*Optics for EUV, X-Ray, and Gamma-Ray Astronomy VI*], *Proc. SPIE* **8861** (2013).

[6] Ramsey, B., "Optics requirements for x-ray astronomy and developments at the marshall space flight center," *Nuclear Instruments and Methods in Physics Research A* **616** (2012).

[7] Pavlinsky, M., "Status of art-xc / srg instrument," in [*Optics for EUV, X-Ray, and Gamma-Ray Astronomy VII*], *Proc. SPIE* **9603** (2015).

[8] Gubarev, M., "The calibration of flight mirror modules for the art-xc instrument on board the srg mission," in [*Space Telescopes and Instrumentation 2014: Ultraviolet to Gamma Ray*], *Proc. SPIE* **9144** (2014).

[9] Davis (Roche), J., "Active full-shell grazing-incidence optics," in [*Adaptive X-Ray Optics IV*], *Proc. SPIE* **9965** (2016).

[10] Gubarev, M. V., "Calibration of a vertical-scan long trace profiler at msfc," in [*Optical Manufacturing and Testing IV*], *Proc. SPIE* **4451** (2001).

[11] Daly, J., "Adhesive bonds for optics: analysis and trade-offs," in [*Optomechanical Engineering*], *Proc. SPIE* **10371** (2017).